The Transition Prediction Toolkit: LST, SIT, PSE, DNS and LES

Thomas A. Zang*
NASA Langley Research Center, Hampton, VA
Chau-Lyan Chang,†
High Technology Corporation, Hampton, VA
and
Lian L. Ng,‡
Analytical Services & Materials Inc., Hampton, VA

Abstract

The e^N method for predicting transition onset is an *amplitude ratio* criterion that is on the verge of full maturation for three-dimensional, compressible, real gas flows. Many of the components for a more sophisticated, *absolute amplitude* criterion are now emerging: receptivity theory, secondary instability theory, parabolized stability equations approaches, direct numerical simulation and large-eddy simulation. This paper will provide a description of each of these new theoretical tools and provide indications of their current status.

1 Introduction

Robust tools for predicting the location of the onset of transition in boundary layers on aerospace vehicles have obvious technological importance. For practical engineering purposes one desires a prediction tool which is quantatively and not just qualitatively correct: the issue is not *whether* transition occurs but *where*. At present transition prediction tends to be based on simple correlations, such as crossflow Reynolds number or Re_θ/M; modified one- or two-equation turbulence models which seek to translate the freestream turbulence level into computations of laminar-transitional-turbulent flow; and linear stability theory.

The pioneering work of Smith & Gamberoni [1] and Van Ingen [2] introduced an empirical method for estimating the location of transition onset based on an *amplitude ratio* criterion. This tool has come to be known as the e^N method or the N-factor method. The next level of transition prediction methodology is likely to involve an *absolute amplitude* criterion. In order to achieve this goal, many more physical effects must be taken into account and more analysis tools must be utilized.

The seeds of transition are the disturbance environment in which the vehicle operates. Transition is born by the receptivity process in which the background disturbances are incorporated within the boundary layer as linear instability waves. It is nurtured by a relatively long region of linear instability growth. Once secondary instability effects develop, they induce rapid growth, and at a sufficiently high amplitude the nonlinear regimes are entered and transition commences, as signified by, say, the skin friction or heat transfer rise.

Characterization of the disturbance background is a prerequisite for an absolute amplitude criterion. Both amplitude and spectral information are required. This is necessarily an experimental task and will not be addressed further in this paper.

The theoretical and computational tools which can now be brought to bear on the transition problem include Receptivity Theory, Linear Stability Theory (LST), Secondary Instability Theory (SIT), Parabolized Stability Equations approaches (PSE), Direct Numerical Simulation (DNS), and Large-Eddy Simulation (LES).

Receptivity theory is a very active area of current research. The essential problem is that the freestream disturbances often have much longer length scales than the instability waves in boundary layers. Therefore, the incorporation of background disturbances into boundary-layer instability waves requires a wavelength conversion mechanism. A variety of linear and asymptotic techniques have been applied to this problem. We refer the reader to [3]-[8] for some recent work in this field. The latter two articles are particularly concerned with compressible flow.

This paper furnishes a brief description of the remainder

*Senior Research Scientist
†Research Scientist.
‡Research Scientist. Present Address: Boeing Commercial Airplane Group, Seattle, Washington.

of these tools and provides examples of recent work. We shall limit ourselves to illustrating these methods for supersonic flows, and shall highlight some recent results from the theoretical and computational transition program at the NASA Langley Research Center.

2 Governing Equations

The starting point for these analysis tools is, of course, the compressible Navier-Stokes equations. In dimensionless form the equations for a thermally and calorically perfect gas are

$$\begin{aligned} \frac{\partial \rho}{\partial t} + \frac{\partial(\rho u_k)}{\partial x_k} &= 0 \\ \frac{\partial u_k}{\partial t} + \frac{\partial(u_k u_l)}{\partial x_l} &= -\frac{1}{\rho}\frac{\partial p}{\partial x_k} + \frac{1}{\rho\, Re}\frac{\partial \sigma_{kl}}{\partial x_l} \\ \frac{\partial p}{\partial t} + u_k\frac{\partial p}{\partial x_k} + \gamma p\frac{\partial u_k}{\partial x_k} &= \frac{1}{M_e^2 Pr Re}\frac{\partial q_k}{\partial x_k} + \frac{\gamma-1}{Re}\Phi \\ \gamma M_e^2 p &= \rho T, \end{aligned} \tag{1}$$

where

$$\sigma_{kl} = -\frac{2}{3}\mu\frac{\partial u_m}{\partial x_m}\delta_{kl} + \mu\left(\frac{\partial u_k}{\partial x_l} + \frac{\partial u_l}{\partial x_k}\right) \tag{2}$$

is the viscous stress tensor,

$$q_k = \kappa\frac{\partial T}{\partial x_k} \tag{3}$$

is the heat flux, and

$$\Phi = \frac{\partial u_k}{\partial x_l}\sigma_{kl} \tag{4}$$

is the viscous dissipation. The Reynolds number is denoted by Re, the Prandtl number by Pr, the Mach number at the boundary-layer edge by M_e, and the ratio of specific heats by γ. (For all the examples in this paper $\gamma = 1.4$.) In these equations ρ is the density, $\mathbf{u} \equiv (u_1, u_2, u_3) = (u, v, w)$ the velocity, p the pressure, and T the temperature. We shall denote the solution vector by $\mathbf{q} = (\rho, u, v, w, p)$. The coordinate system is chosen so that $\mathbf{x} \equiv (x_1, x_2, x_3) = (x, y, z)$, where x, y, and z are the streamwise, spanwise, and wall-normal coordinate directions, respectively.

In this paper, most dependent variables are normalized with respect to their boundary-layer edge values; p is scaled by $\rho_e^* u_e^{*2}$. Distances are scaled by the variable $L^* = (\nu_e^* x^*/u_e^*)^{1/2}$. The superscript * characterizes a dimensional quantity, the subscript e indicates a value at the edge of a boundary layer, u is the streamwise velocity, and ν is the kinematic viscosity. The viscosity, μ^*, is assumed to be given by the Sutherland formula.

Although results will be presented here for flat plates, cylinders and cones, the equations and notation will be given just for the flat plate. See [9] for the appropriate equations for the more general situation.

3 Linear Stability Theory

The techniques of compressible linear stability theory are quite well know; see, for example, [10]. The starting point is a laminar mean flow, $\mathbf{q}_0$. In most cases an approximate mean flow is utilized, e.g., a quasi-parallel solution of the boundary-layer equations. One must then imagine that an appropriate forcing term has been added to Eq. (1). See [11] for a recent discussion. The total flow field, $\mathbf{q}(\mathbf{x}, t)$, is written as

$$\mathbf{q}(\mathbf{x}, t) = \mathbf{q}_0(z) + A\left(\mathbf{q}_1(z)e^{i(\alpha x + \beta y - \omega t)} + \text{c. c.}\right). \tag{5}$$

The streamwise and spanwise wave numbers are denoted by α and β, respectively, and ω is the (temporal) frequency. The complex amplitude function, $\mathbf{q}_1(z)$, determines the structure in the wall-normal direction. The compressible Navier-Stokes equations are then linearized about the mean flow to first-order in the amplitude A. When combined with appropriate boundary conditions, an eigenvalue problem results.

The spanwise wavenumber is invariably taken to be real. In temporal theory, α is real and ω is the (complex) eigenvalue, with ω_i the spatial growth rate. In the spatial concept, ω is real and α is the eigenvalue, with $-\alpha_i$ the spatial growth rate. In many cases the simpler temporal theory is applied, and the spatial growth rate approximated by $-\alpha_i = \omega_i/c_g$, where c_g is the group velocity of the wave. The linear instability is referred to as the *primary* instability.

Some recent developments for compressible flow include incorporation of non-parallel effects through multiple-scale techniques [12], real gas effects [13], proper shock-wave boundary conditions [14], and clarification of some issues regarding propagation of three-dimensional waves [15].

The N-factor method is applied by first computing the laminar mean flow past the body of interest and then applying LST to that flow. For a given frequency, ω, the streamwise location at which a wave first becomes unstable, x_0, is identified and then the spatial growth rate is integrated downstream to produce the N-factor: $N(\omega) = \int_{x_0}^{x}(-\alpha_i)dx'$. (Note that if the amplitude of the instability at x_0 is denoted by A_0, then the amplitude at x is given by $A/A_0 = e^{N(\omega)}$; thus, $e^{N(\omega)}$ measures the amplitude ratio.) This calculation is performed for a range of frequencies, and for each x, the maximum over ω, denoted

by just N, is taken.

The estimate of transition onset is based upon an empirical correlation between N and the location of transition. The N-factor method has had a surprising degree of success, even considering its limitations, such as inapplicability to flows in a high disturbance background for which the linear instability regime is "by-passed". The N-factor method has matured to the point at which an analysis capability is imminent for transition estimation across the speed range (including real gas effects) and for arbitrary steady three-dimensional mean flows.

The computer requirements for solving a single LST eigenvalue problem are inconsequential. Even application of the N-factor method to a three-dimensional mean flow requires only on the order of an hour of supercomputer time. However, a non-trivial related task is computation of an accurate mean flow. LST requires accurate (and oscillation-free) mean flows and this is a far more stringent requirement than is customary in conventional steady-state CFD. This can take many tens of supercomputer hours for a three-dimensional configuration.

4 Secondary Instability Theory

Secondary instability theory picks up where LST leaves off. In SIT one includes some weakly nonlinear (and three-dimensional) effects. One considers the linear stability with respect to secondary disturbances of a base flow comprised of a laminar mean flow (assumed locally parallel) modulated by a small (but finite) amplitude primary disturbance. SIT is now well-established for incompressible flow. See Herbert [16] for a thorough review of the subject. In recent years it has been extended and applied to compressible boundary layers in [17], [18], [19], and [20]. Here we review some of the developments discussed in [20].

The frequency, wavelength, and shape of the primary disturbance are obtained using LST. The primary wave is assumed to have no growth during the evolution of the secondary disturbance. In a Galilean frame, $x^+ = x - c_r t$, moving with the phase velocity, c_r, of the primary wave, the total flow variable, $\mathbf{q}$, can be written in the Floquet form

$$\mathbf{q} = \mathbf{q}_b + \epsilon \Re\left\{ e^{\sigma t} e^{\gamma x^+} e^{i\beta_2 y} e^{ih\frac{\alpha_1}{2}x^+} \sum_{j=-\infty}^{\infty} \mathbf{q}_{2,j}(z) e^{ij\alpha_1 x^+} \right\}, \tag{6}$$

where $\mathbf{q}_b$ is given by Eq. (5). Hereafter, the subscripts 0, b, 1, and 2 refer, respectively, to the laminar mean flow, the modulated base flow, the primary disturbance, and the secondary disturbance. The primary wave amplitude, A, is defined so that it corresponds to the maximum value of the perturbation mass flux. The equations governing the secondary disturbance are obtained by linearizing Eq. (1) about the modulated base flow. The discretized disturbance equations are converted into a complex algebraic eigenvalue problem for σ or γ and their associated eigenfunctions. In temporal theory, $\gamma = 0$ and $\sigma \neq 0$ is the complex eigenvalue to be determined. In the spatial concept, we write $\sigma = \gamma c_r$ in Eq. (6) and solve for γ as the eigenvalue [16]. The temporal and spatial growth rates are given by the real parts of σ and γ, respectively. The detuning parameter, h, defines the type of secondary instability. The subharmonic modes are given by $h = 1$, while the fundamental modes correspond to $h = 0$. In practice the sum in Eq. (6) includes from 2 to 5 modes.

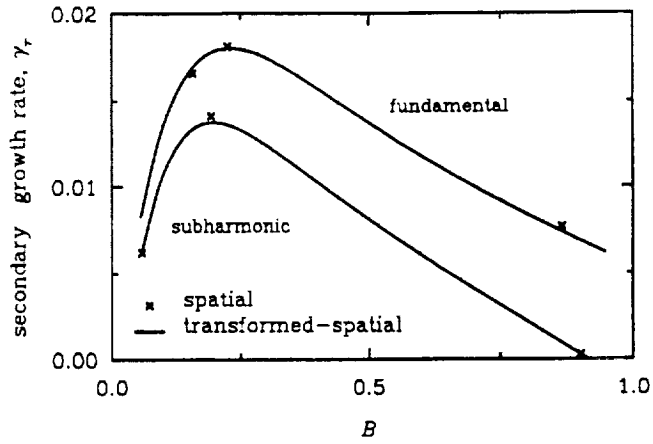

Figure 1: Variation of γ_r with B when $M_e = 1.6$. Fundamental at $A = 2.9\%$. Subharmonic at $A = 1.5\%$.

As one example, consider the boundary layer over an insulated flat plate at Mach number $M_e = 1.6$, Reynolds number $Re = 1050$, Prandtl number $Pr = 0.72$, and temperature $T_e = 216^0$ Rankine. The primary wave is slightly damped, and is located near branch two of the neutral stability curve with $\alpha_1 = 0.1471$ and $F \equiv 10^6 \times \omega_1/Re = 82.6$. For clarity, the secondary growth rate obtained from the temporal theory, which has been converted to a spatial growth rate by using the transformation $\gamma_r = \sigma_r/c_r$, is termed the "transformed-spatial" growth rate. In many cases of interest both the dominant fundamental and subharmonic travel synchronously with the primary, i.e., $\gamma_i = 0$.

In Fig. 1, the secondary growth rate is plotted as a function of the normalized spanwise wavenumber $B \equiv 10^3 \times \beta_2/Re$. (For constant boundary-layer edge conditions, the parameter B signifies a wave of fixed spanwise wavelength as it propagates downstream.) The "transformed-spatial" growth rate agrees well with the (true) spatial growth rate. The most amplified subhar-

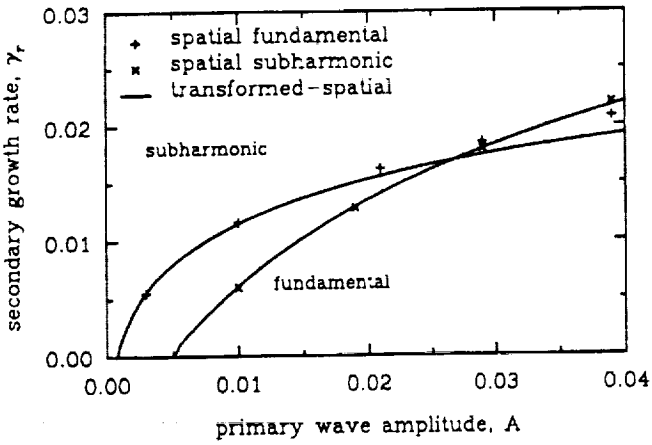

Figure 2: Variation of γ_r with A when $M_e = 1.6$.

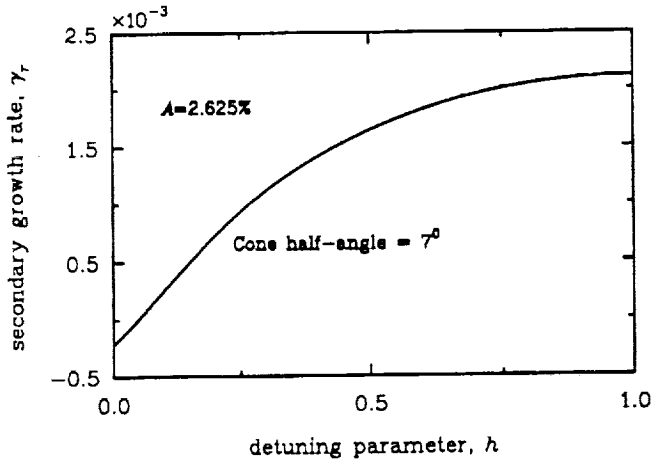

Figure 3: Effect of the detuning parameter on γ. $M_e = 6.8$ and $B = 0.135$.

monic disturbance consists of a pair of oblique waves traveling at equal and opposite angles at about 70^0 to the mean-flow direction. The most unstable fundamental disturbance is comprised of a stationary mode, which represents a spanwise periodic distortion of the mean flow, and a pair of oblique waves propagating in opposite directions at about 57^0 to the mean-flow direction.

Figure 2 depicts the typical catalytic effect of the primary amplitude on the growth rates of the secondary disturbances. The spanwise wavenumbers, B, of the subharmonic and the fundamental are 0.19 and 0.22, respectively; these particular values of B correspond roughly to the most amplified secondary disturbances. The subharmonic instability prevails over the fundamental instability in an environment with a primary amplitude, A, of less than about 2.8%, while the converse is true for higher values of A. The transformed-spatial growth rates of the subharmonic modes are almost identital to the spatial rates for small A — the former increasingly underpredicts the latter as A increases from 1.5%.

The preceding behavior is expected, since the use of temporal data to approximate spatial growth becomes less accurate when the growth rate is relatively high. Still, the transformation of temporal data to approximate the spatial growth rates of fundamental resonance modes is surprisingly accurate even for a primary amplitude as high as 4%.

The second example, given in Fig. 3, corresponds to a laminar boundary layer on an insulated 7-degree half-angle sharp cone at $M_e = 6.8$. The parameters are $Re = 1939$, $T_e = 128^0$ Rankine, $Pr = 0.70$. The primary disturbance is axisymmetric and is of the "second mode" type with $\alpha_1 = 0.2788$ and $F = 135$. The two sets of calculations also serve to contrast the secondary instability arising from a first-mode primary (at $M_e = 1.6$) with that arising from a second-mode primary (at $M_e = 6.8$). Over a range of Mach numbers up to at least 6.8, subharmonic secondary instability ($h = 1$) is found to prevail in a low primary-disturbance environment. This is especially true for high-speed flows. In particular, as illustrated in Fig. 3, no fundamental instability ($h = 0$) for $M_e = 6.8$ exists even for a primary amplitude of 2.625%. In fact, both the first- and second-mode primary waves associated with high-speed flows have been found ineffective in catalyzing unstable fundamental resonance modes.

Recent developments in SIT include incorporation of non-parallel effects (but only for for the evolution of the primary wave) [17]. Ng & Erlebacher [19] have developed a fairly general capability which allows for oblique primary waves (important at low supersonic Mach number, where the most unstable primary is oblique).

SIT has greater computational requirements than LST – the matrix eigenvalue problems which must be solved are larger than in LST. Nevertheless, a solution can be obtained in minutes on a supercomputer.

5 Parabolized Stability Equations

As a consequence of the rapid growth of the secondary wave, many harmonic waves, including the mean flow correction mode, are excited to large amplitudes, and eventually strongly nonlinear effects ensue; the flow then becomes transitional. Although SIT furnishes a guide to mechanisms that may be present near transition onset, it does not at present account for many non-parallel effects, and it incorporates only the lowest level non-linearity.

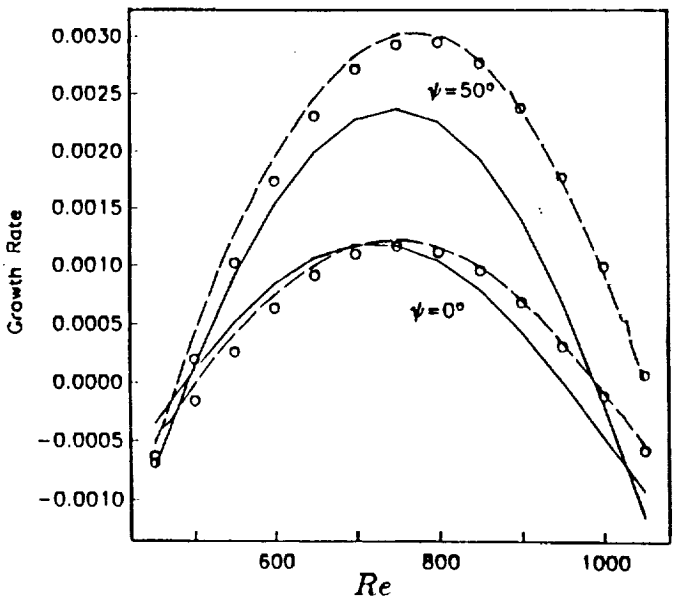

Figure 4: PSE computation of the effect of non-parallel mean flows for both 2-D and 3-D disturbances of a M_e = 1.6 flow at $F = 40$. (Solid lines are from parallel LST, dashed lines from PSE calculations, and symbols are from multiple-scales analysis [12].)

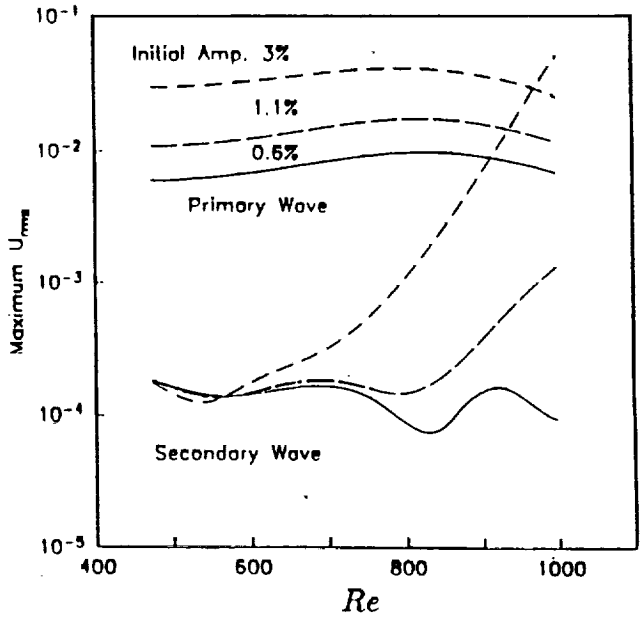

Figure 5: PSE amplitude evolution of the primary and subharmonic waves at $M_e = 1.6$, $F = 50$, and $B = 0.053$.

One efficient method which does incorporates both non-parallel and non-linear effects is the parabolized stability equations approach, first suggested by Herbert and Bertolotti [21], [22]. The PSE method facilitates the solution of the full partial differential equations for the disturbances by employing a partial parabolization along the dominant flow direction. In this approach, the disturbance is decomposed into a wave part and a shape function part. The elliptic terms are retained for the wave part, whereas the governing equations for the shape function are parabolized in the streamwise direction. The parabolized equations for the shape function are then solved numerically by a marching procedure. The wave properties are extracted from a local analysis. Nonlinear terms are formulated as forcing functions for the corresponding linear equations. Because the equation set contains non-parallel as well as nonlinear terms, the PSE method governs the spatial evolution of disturbances from the linear stage up to the transitional stage.

The PSE approach has been successfully applied to the stability of supersonic two-dimensional boundary layers by Bertolotti & Herbert [23] and Chang *et al.* [24]. In the linear regime, the method provides a means to include non-parallel effects due to the growth of the boundary layer, which is ignored in traditional LST. Furthermore, non-linear effects such as wave/wave interaction or secondary instability can be simulated by the non-linear PSE.

To demonstrate the applicability of the PSE approach, we present some of the results given in [24]. Linear PSE calculations were performed for a Mach 1.6 flat-plate boundary layer previously studied by El-Hady [12]. The frequency of the disturbances is $F = 40$. Calculations were performed for both 2-D and 3-D linear disturbances; the wave angle for the oblique, 3-D waves was about 50°. The growth rate of the mass flow fluctuations from the PSE calculations together with the multiple-scales results are plotted along with the growth rates obtained by quasi-parallel LST in Fig. 4. PSE results agree quite well with those obtained from the multiple-scales approach. The results also indicate that for the first mode disturbance at Mach 1.6, flow non-parallelism has more effect on three-dimensional disturbances than on two-dimensional ones. The non-parallel effect on oblique waves is qualitatively very similar to that in incompressible flows, as found by Bertolotti [21].

Compressible non-linear PSE computations for secondary instability mechanisms and the subsequent start of laminar breakdown have also been demonstrated . The flow is again a Mach 1.6 flat-plate boundary layer with a primary disturbance frequency of $F = 50$. The free-stream temperature is 540° Rankine and the Prandtl number is $Pr = 0.71$. Figure 5 shows the evolution of primary and subharmonic disturbances for various initial amplitudes of

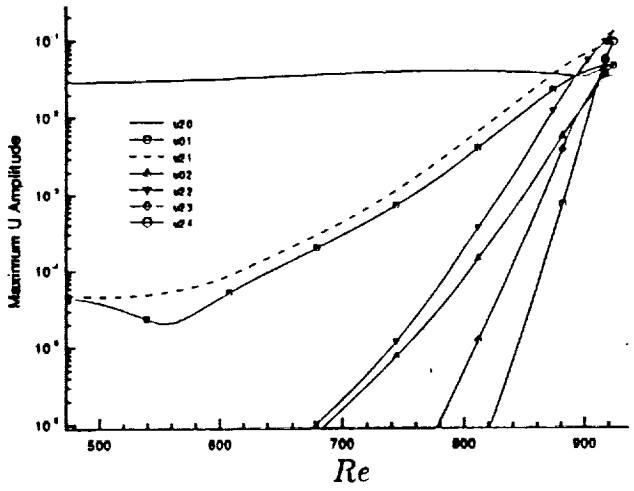

Figure 6: PSE amplitude evolution of various Fourier modes for a $M_e = 1.6$ fundamental breakdown

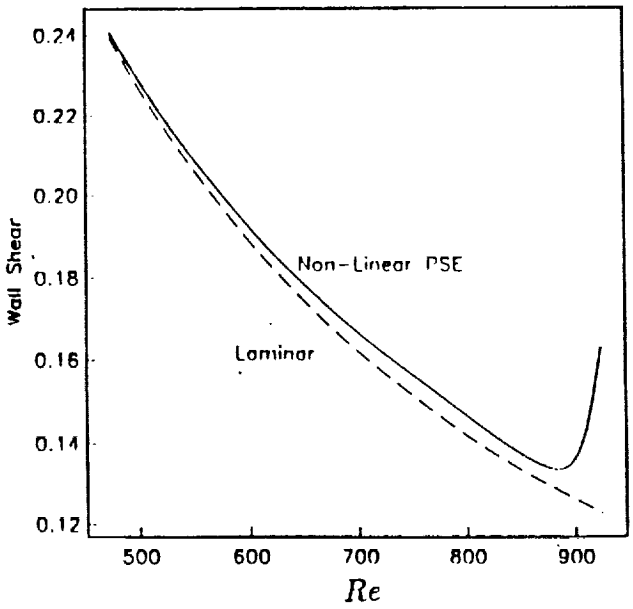

Figure 7: PSE wall shear of laminar and perturbed flows for a $M_e = 1.6$ fundamental breakdown.

the primary waves (the subharmonic amplitudes are the same for all three cases). The spanwise wave number of the subharmonic mode is fixed at $B = 0.053$, which corresponds to an oblique wave angle of 45°. As can be seen, a 1.1% initial amplitude for the primary mode is enough to trigger the secondary growth.

Non-linear PSE calculations were also performed for the same Mach 1.6 case but for a fundamental-type secondary resonance. The initial amplitude of the primary wave is again 3% and that of the secondary is taken to be 0.005%. The spanwise wave number is $B = .152$ (oblique wave angle of 60° for the secondary wave) and the primary wave frequency is again $F = 50$. The non-linear evolution of the maximum rms amplitude of u' (a prime is used to denote the fluctuating part of a variable) is shown in Figure 6. Clearly, the presence of the primary 2-D and secondary 3-D disturbances results in wave resonance and strong secondary growth of the oblique wave. When the secondary disturbance is amplified to about the same amplitude of the primary wave, all harmonics are excited and the flow becomes transitional. This is confirmed by plotting the average wall shear in Figure 7. The computed wall shear is only slightly above the laminar value for most of the computational domain. (The PSE wall shear lies above the laminar value right from the beginning because of the relatively high initial amplitude of the 2-D primary disturbance.) Eventually the wall shear departs sharply from the laminar value, indicative of transition onset. Thus, the PSE computation captures the skin friction rise, which is one of the criteria for transition onset; accurate prediction of its location is a prime goal of transition prediction methods.

Linear PSE computations (equivalent to non-parallel LST) are quite cheap. Nonlinear PSE can compute up to the skin friction rise in no more than an hour of supercomputer time. However, current numerical techniques for nonlinear PSE have computational requirements which scale quadratically with both the number of spanwise Fourier components and the number of temporal frequencies retained in the approximation. This means that PSE computations for the later stages of transition and for random inflow and/or freestream conditions are exceedingly expensive.

The SIT and PSE tools that have been described up to this point are oriented towards *forced* transition, i.e., transition characterized by sharply defined frequencies as might occur from specific forcing. The technologically interesting problem is that of *natural* transition, for which a broad range of frequencies is present. To capture the nonlinear interaction between a wide range of frequencies, DNS and LES are currently the most appropriate tools.

6 Direct Numerical Simulation

Direct numerical simulation solves the time-dependent, three-dimensional, nonlinear, Navier-Stokes equations subject to prescribed initial and boundary conditions without recourse to empirical models. A thorough review of this approach has been given by Kleiser & Zang [25].

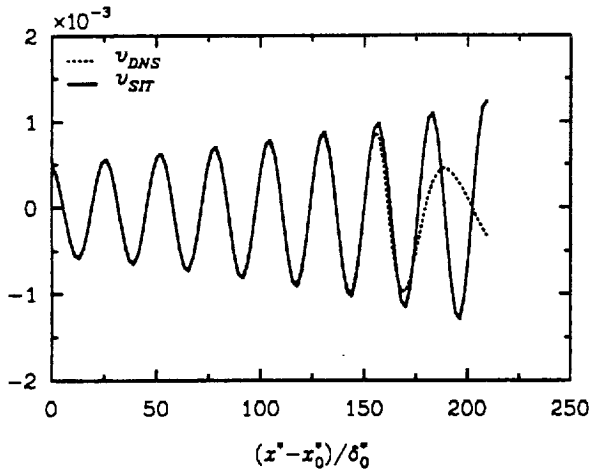

Figure 8: Spatial SIT vs. DNS for a $M_e = 1.6$ fundamental instability.

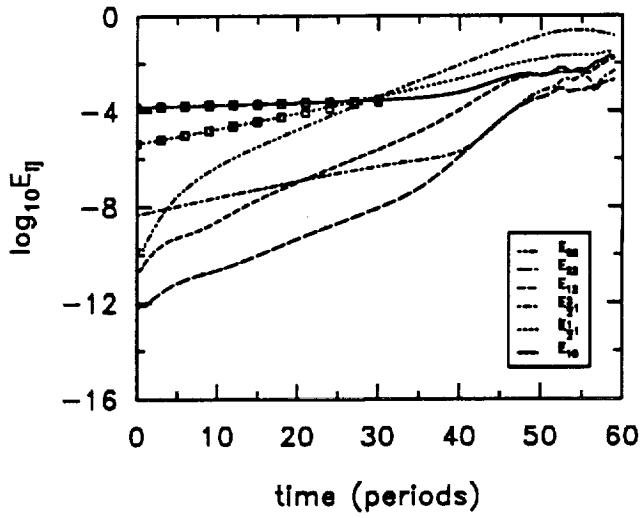

Figure 9: Evolution of selected harmonics from DNS of $M_e = 4.5$ cylinder subharmonic transition.

When attacked as the total boundary-layer transition problem – from receptivity through fully-developed turbulence – the non-parallel, spatial formulation is certainly more appropriate than the temporal approximation. However, DNS for the complete transition process is an exceedingly expensive tool even for the low Reynolds numbers to which it is of necessity restricted. Gilbert & Kleiser [26] performed the first well-resolved simulation of the complete transition to turbulence and this took several hundred supercomputer hours for a temporal computation of forced incompressible transition. With somewhat relaxed resolution requirements Rai & Moin [27] have recently computed bypass transition for low-speed flow past a flat plate. This required many hundreds of supercomputer hours and it remains to be seen what the requirements are for a well-resolved computation for this problem. For the foreseeable future, both temporal and spatial DNS have a role, but this tool ought to be applied selectively.

One role for DNS is the corroboration of simpler tools, such as SIT and PSE. For compressible flows it has been used to verify temporal SIT [19], [9], spatial SIT [20], and some aspects of nonlinear PSE [24]. Given the algebraic complexity of SIT and PSE, particularly for oblique primaries, this role is a needed one to establish confidence in them. (It also furnishes a stringent calibration of DNS.)

One comparison between spatial (but quasi-parallel) SIT and DNS by Ng & Zang [20] was performed for a fundamental type instability at $M_e = 1.6$, $Re = 613$, $Pr = 0.70$, and $T_e = 520^0$ Rankine. The primary wave is a 2-D first mode with frequency $F = 73$. The subharmonic secondary wave has spanwise wavenumber $B = 0.1465$. The amplitude of the primary is chosen to be 6%, while that of the secondary is 0.1%. Although the spatial DNS code is designed for non-parallel flow, for comparison with the quasi-parallel SIT theory the mean flow was constrained to be parallel by using a forcing function. The initial conditions consisted solely of the laminar mean flow. At the inflow boundary, $x^* = x_0^* = u_e^* L^{*^2}/\nu_e^*$, the flow consisted of the mean flow plus the appropriate contributions from the linear and secondary eigenfunctions. The physical domain consisted of 8 wavelengths of the primary wave, with "buffer domain" modifications [28] to the Navier-Stokes equations in the last 2 wavelengths used to ameliorate potential difficulties with the outflow boundary conditions. (See [20] for details.) Figure 8 shows the spanwise velocity component, v, at $z = 0.2\delta^*$, where δ^* is the displacement thickness, and $\beta_2 y = \pi/2$ after 10 periods of forcing; this component is due solely to the secondary instability. The agreement between the DNS and SIT results is excellent, except, of course, in the buffer domain.

This computation utilized 12 points per streamwise wavelength. For transition in high-speed flows the growth rates of both primary and secondary disturbances are lower than for incompressible flow. As a consequence on the order of 10^2 wavelengths would be needed to follow the primary/secondary stages from about the 1% level to the skin friction rise. This is a prohibitive expense and argues strongly for the use of simpler methods such as SIT and especially PSE for routine application to the early stages of transition.

The unique niche for DNS is the highly nonlinear, laminar breakdown stage and the subsequent transition to turbulence; for this the non-parallel effects appear to be less significant than they are for the rather lengthy primary and secondary instability stages. These early stages are nowadays treated far more efficiently by SIT and PSE ap-

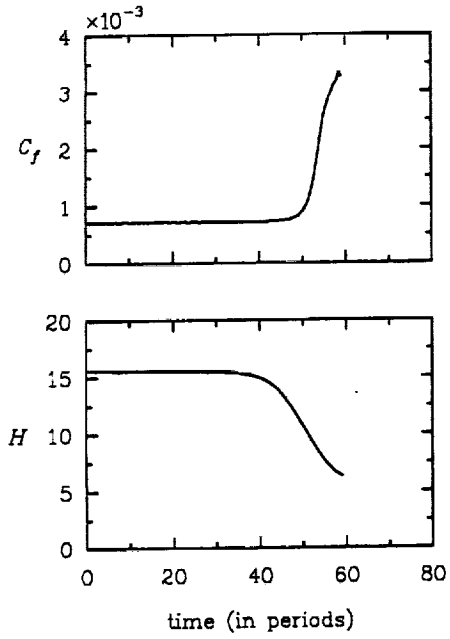

Figure 10: Skin friction and shape factor from DNS of $M_e = 4.5$ cylinder subharmonic transition.

proaches than by DNS. Indeed, the simpler theories can well be used to set the stage for the DNS: LST selects the dominant primary instability (and determines the relevant streamwise scales); SIT and/or PSE select the dominant spanwise scales and can be used to "jump start" the DNS at fairly high disturbance levels.

This is the approach that was taken by Pruett & Zang [29] in their temporal DNS of transition in Mach 4.5 flow past a cylinder. The primary disturbance was a second mode and the secondary disturbance was of subharmonic type. Due to the periodicity assumptions in the streamwise (x) and spanwise (y) directions, the dependent variables have Fourier series representations in these directions. A useful measure of the strength of a given Fourier harmonic is

$$E_{k_x,k_y}(t) = d_{k_x} d_{k_y} \int_0^\infty \rho_0(z) |\hat{\mathbf{u}}_{k_x,k_y}(z,t)|^2 dz, \quad (7)$$

where $\hat{\mathbf{u}}_{k_x,k_y}$ is the Fourier coefficient of the velocity corresponding to wavenumbers k_x and k_y (with respect to α_1 and β_2, respectively;

$$d_k = 2 - \delta_{k0} \quad (8)$$

accounts for some of the symmetries in the problem. The quantity E_{k_x,k_y} is approximately the kinetic energy of the (k_x, k_y) mode.

Figure 9, taken from [29], summarizes the time evolution of the principal modes for the Mach 4.5 cylinder simulation. (Time is reckoned in units of the period of the primary wave.) The DNS proceeded through the stages of primary/secondary instability then underwent weakly nonlinear and strongly nonlinear stages, and finally commenced laminar breakdown. The stages cited above last from 0-15, 15-35, 35-45 and 45-60, respectively. The symbols on the figure are the predictions from LST and SIT for the growth of the primary and secondary disturbances. They are in good agreement with the DNS. One interesting feature of this simulation is the prominence that the $(0,2)$ mode assumes in the latter stages of transition. This mode is not present in the initial conditions (nor in SIT) and is generated by nonlinear effects. Additional DNS have revealed that this mode plays an essential role in the final laminar breakdown.

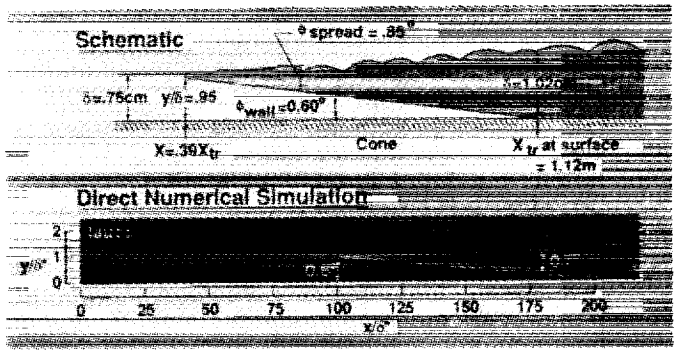

Figure 11: Cartoon of the precursor transition effect (top) [30] and its manifestation in the spatially-reconstructed Reynolds stress from DNS of $M_e = 6.8$ cone subharmonic transition (bottom).

Figure 10 shows the evolution of the skin friction, C_f, and the shape factor, H, for the Mach 4.5 cylinder transition. This simulation was stopped at about 60 periods because of strong gradients that even its million grid points could not resolve. Indeed, the judgment of Pruett & Zang [29] was that the resolution became questionable after 55 periods. This resolution problem intensifies as Mach number increases, and in a particular computation may eventually manifest itself in negative values of some of the thermodynamic quantities. This particular difficulty does not arise for low-speed DNS. For compressible flow the dilemma is that highly-accurate central-difference schemes do not have sufficient artificial viscosity to resolve strong gradients at high Reynolds number, whereas conventional upwind CFD schemes are so dissipative that they corrupt the delicate physics of transition. An encouraging recent development is the work of Atkins [30], which demonstrated good results for a compressible free shear layer transition using a fifth-order ENO scheme.

The shape factor plot suggests that the simulation

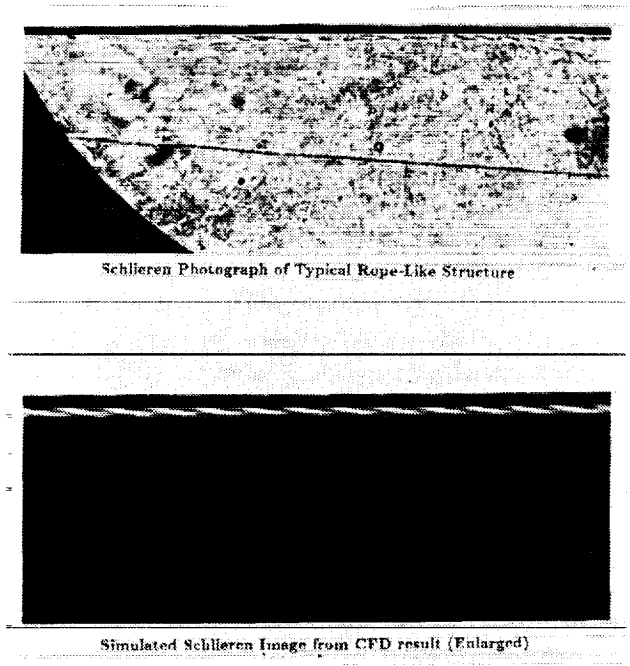

Figure 12: Experimental (top) [32] and DNS (bottom) [25] visualizations of the rope-like structures in supersonic transition.

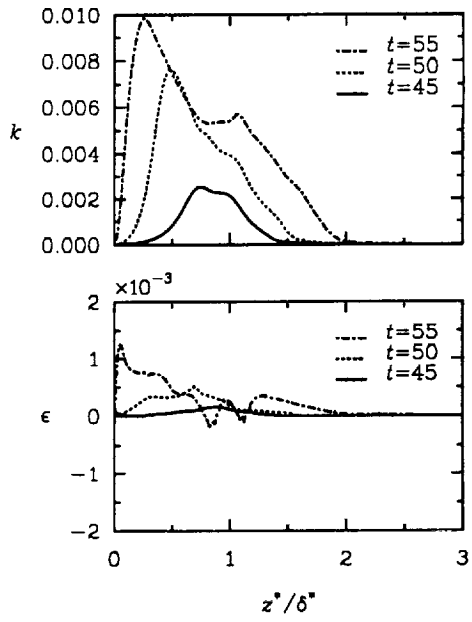

Figure 13: Evolution of turbulent kinetic energy and dissipation for $M_e = 4.5$ cylinder subharmonic transition.

has proceeded almost completely through the transition process. Figure 11 presents the spatially-reconstructed streamwise velocity fluctuations, as represented by the Reynolds-stress component $\tau_{11} = -\overline{\rho u'u'}$, from a Mach 6.8 cone simulation [29]. These exhibit the so-called "precursor transition effect", sketched in the cartoon in the top part of the figure, whereby the transition originates near the boundary-layer edge and gradually propagates toward the wall. This same effect is present in the DNS. Flowfield visualizations presented in Fig. 12 demonstrate the presence in the Mach 4.5 cylinder DNS of the "rope-like structures" that have been observed in numerous experiments ([31],[32], [33]). One of the more significant conclusions of [29] was that the rope-like structures are actually manifestations of SIT and not LST, as had long been suspected.

A last sample of results from this DNS is presented in Fig. 13. It illustrates the evolution of the turbulent kinetic energy, k, and the turbulent dissipation, ϵ, through the transition region. This kind of information, supplemented by detailed information on the key terms in the evolution equations for these quantities, has the potential to lead to substantial improvements in two-equation models for transitional flow. However, DNS (particularly spatial DNS) is so computationally intensive that a less drastic, but still effective, tool for exploring the later stages of transition would be quite desirable. The following section describes a promising candidate.

7 Large-Eddy Simulation

In large-eddy simulation the small *scales* of the flow are modeled in terms of the large-scale flow. The Reynolds-averaged Navier-Stokes equations, in contrast, model the higher-order *moments* in terms of the lower-order moments. In LES the flow variables are decomposed into a large-scale (resolvable) component and a small-scale (subgrid–scale) component. LES was originally developed for turbulent flow (see [34] for a survey of the state-of-the-art in LES), and, at least with the more established subgrid-scale (SGS) models, some refinements have proven necessary to handle transitional flow properly. In the transitional case one not only wants to have a model which works well for the final turbulent state, but also one which captures the primary, secondary and nonlinear stages correctly (without, for example, exerting excessive damping of the instability waves), predicts well the location of transition onset, and makes good predictions from transition onset through the transitional zone to the fully turbulent state. Piomelli and co-workers ([35], [36], [37], [38]) have led the effort to utilize DNS of transition to calibrate and refine SGS models for this process. This work has to date been confined to incompressible flow. In this section we describe some recent developments for compressible transition modeling via LES.

The large-scale field is defined by the filtering operation:

$$\overline{\mathcal{F}}(\mathbf{x}) = \int G(\mathbf{x},\mathbf{x}')\mathcal{F}(\mathbf{x}')\lceil\mathbf{x}', \tag{9}$$

where the integral is extended over the entire spatial domain and $G = \overline{G}_1\overline{G}_2\overline{G}_3$, where $\overline{G}_i(x_i)$ is the filter function in the ith direction. For the velocity and temperature, Favre filtering is utilized: $\mathcal{F} = \tilde{\mathcal{F}} + \mathcal{F}'$, where $\mathcal{F}'$ is the SGS part of $\mathcal{F}$ and the Favre filter is defined by $\tilde{\mathcal{F}} = \overline{\rho\mathcal{F}}/\overline{\rho}$. The sharp Fourier cutoff filter is chosen for this work because of previous experience with this filter in LES of incompressible transition ([35]).

The dimensionless governing equations for compressible LES are

$$\frac{\partial\overline{\rho}}{\partial t} + \frac{\partial(\overline{\rho}\tilde{u}_k)}{\partial x_k} = 0$$

$$\frac{\partial(\overline{\rho}\tilde{u}_k)}{\partial t} + \frac{\partial(\overline{\rho}\tilde{u}_k\tilde{u}_l)}{\partial x_l} = -\frac{\partial\overline{p}}{\partial x_k} + \frac{\partial\overline{\sigma}_{kl}}{\partial x_l} + \frac{\partial\tau_{kl}}{\partial x_l}$$

$$\frac{\partial\overline{p}}{\partial t} + \tilde{u}_k\frac{\partial\overline{p}}{\partial x_k} + \gamma\overline{p}\frac{\partial\tilde{u}_k}{\partial x_k} = \frac{1}{M_e^2 PrRe}\frac{\partial\overline{q}_k}{\partial x_k}$$

$$+\frac{\gamma-1}{Re}\overline{\Phi} + \frac{1}{M_e^2}\frac{\partial Q_k}{\partial x_k} + (\gamma-1)\overline{u_k\frac{\partial p}{\partial x_k}} - (\gamma-1)\tilde{u}_k\frac{\partial\overline{p}}{\partial x_k}$$

$$\gamma M_e^2\overline{p} = \overline{\rho}\tilde{T}\,. \tag{10}$$

The SGS stress tensor τ_{kl} and the SGS heat flux Q_k are defined by $\tau_{kl} = -\overline{\rho}(\widetilde{\tilde{u}_k\tilde{u}_l} - \tilde{u}_k\tilde{u}_l + \widetilde{u_k'\tilde{u}_l} + \widetilde{u_l'\tilde{u}_k} + \widetilde{u_k'u_l'})$ and $Q_k = -\overline{\rho}(\widetilde{\tilde{u}_k\tilde{T}} - \tilde{u}_k\tilde{T} + \widetilde{u_k'\tilde{T}} + \widetilde{\tilde{u}_k T'} + \widetilde{u_k'T'})$.

There have been a number of SGS models proposed for compressible LES ([39],[40], [41],[42]). Two of these models have been applied to the Mach 4.5 transition problem discussed in the preceeding section.

The first SGS model considered is the SEZHu model derived by Speziale *et al.* [40] for compressible isotropic turbulence. This model has been chosen because there are now available some extensive *a posteriori* comparisons of its performance on compressible, isotropic turbulence ([44], [45]). Following the work of Piomelli *et al.* [46], only the Smagorinsky portion of the SEZHu model is used with the Fourier cutoff filter. (This filter is applied in x and y; no filtering is applied in the inhomogeneous z direction.) Hence, the SGS stress model is of the form

$$\tau_{kl} = 2\,C_R\mathcal{D}\Gamma\,\overline{\rho}\,\Delta^2\,II_{\tilde{S}}^{1/2}\left(\tilde{S}_{kl} - \frac{1}{3}\tilde{S}_{mm}\delta_{kl}\right)\,, \tag{11}$$

and the SGS heat flux is given by

$$Q_k = -\frac{C_R\mathcal{D}\Gamma\overline{\rho}}{Pr_T}\Delta^2 II_{\tilde{S}}^{1/2}\frac{\partial\tilde{T}}{\partial x_k}\,, \tag{12}$$

where

$$\mathcal{D} = \left(1 - e^{-z^+/25}\right)^2, \tag{13}$$

$\tilde{S}_{kl} = (\partial\tilde{u}_k/\partial x_l + \partial\tilde{u}_l/\partial x_k)/2$ is the Favre-filtered rate-of-strain tensor and $II_{\tilde{S}} = \tilde{S}_{mn}\tilde{S}_{mn}$ is its second invariant. C_R is the compressible Smagorinsky constant, Pr_T is the turbulent Prandtl number, and $\Delta = (\Delta x\Delta y\Delta z)^{1/3}$. The function Γ is an intermittency-like term that turns itself on slowly in the transitional zone [35]. Eq. (13) represents a Van Driest wall damping and z^+ indicates a wall-normal distance made dimensionless by the wall shear velocity and kinematic viscosity.

The second SGS model considered here is the structure function model [43], which is based on a physical space implementation of the concept of spectral eddy viscosity. Some results for this model have been reported for a spatial LES of a Mach 5 boundary layer [41]. The structure function model is of the following form for the SGS shear stress and heat flux:

$$\tau_{kl} = C_R\mathcal{D}\Gamma\,\overline{\rho}\,\Delta x\sqrt{\overline{F}_2\left(\mathbf{x},\Delta x,\Delta y,t\right)}\times\left(\tilde{S}_{kl} - \frac{1}{3}\tilde{S}_{mm}\delta_{kl}\right) \tag{14}$$

$$Q_k = -\frac{C_R\mathcal{D}\Gamma\overline{\rho}\Delta x}{Pr_T}\sqrt{\overline{F}_2\left(\mathbf{x},\Delta x,\Delta y,t\right)}\frac{\partial\tilde{T}}{\partial x_k}\,, \tag{15}$$

where

$$\begin{aligned}\overline{F}_2 = \;& \tfrac{1}{4}\;\left(||\mathbf{u}(x+\Delta x,y,z,t) - \mathbf{u}(x,y,z,t)||^2\right.\\ &+\;||\mathbf{u}(x,y,z,t) - \mathbf{u}(x-\Delta x,y,z,t)||^2\\ &+\;\frac{\Delta x}{\Delta y}(||\mathbf{u}(x,y+\Delta y,z,t) - \mathbf{u}(x,y,z,t)||^2\\ &+\;\left.||\mathbf{u}(x,y,z,t) - \mathbf{u}(x,y-\Delta y,z,t)||^2)\right)\,.\end{aligned} \tag{16}$$

Although neither Van Driest wall damping nor the intermittency term were in the structure function model as used in [41], they were added here as they seem to furnish better results.

The structure-function SGS model was tested *a posteriori* both with and without the "intermittency" function, and a comparison is given in Fig. 14 for the primary and secondary components. (In the latter case $\Gamma = 1$.) The coefficients for these runs were $C_R = 0.06$, which is the value recommended in [41], and $Pr_T = 0.70$. The LES used 10^4 grid points, two orders of magnitude fewer than the DNS. The original structure function model is clearly far too dissipative in the early stages, whereas the modified model agrees very well with the high-resolution DNS. In this respect these results are similar to those reported in [35] for the original and modified Smagorinsky model when applied to incompressible transition. The integral properties are in quite good agreement with those of the high-resolution DNS up to T = 55; they are summarized

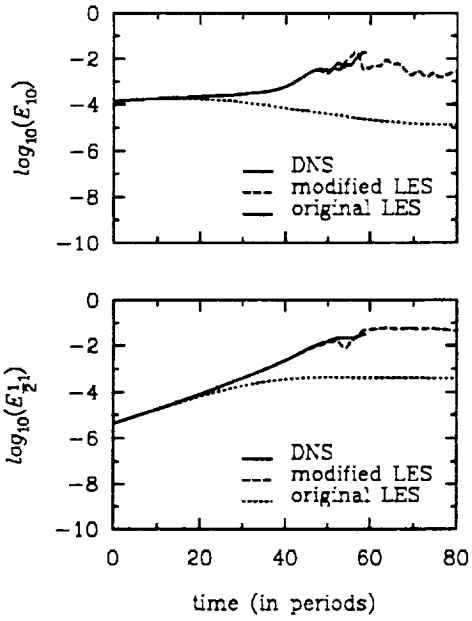

Figure 14: Comparison of unmodified and modified structure function for LES of $M_e = 4.5$ cylinder transition.

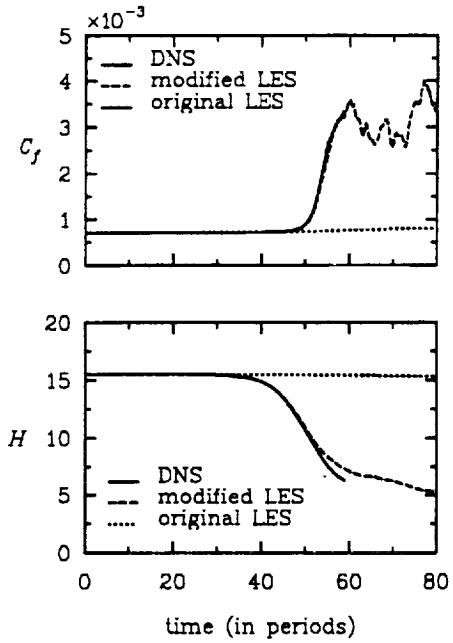

Figure 15: Evolution of skin friction and shape factor for LES of $M_e = 4.5$ cylinder transition.

in Figure 15. Note that the computation reaches the fully turbulent regime.

For the SEZHu model the nominal coefficient is $C_R = 0.011$ [44]. However, on the same grid as was used for the previous LES computations this had to be increased to $C_R = 0.50$ in order to compute all the way through to turbulence. The reason for this is not entirely clear at present. It might be that the larger value of the Smagorinsky constant serves to provide artificial viscosity needed to stabilize the computation, or it might be due to the much smaller length scales involved in second mode transition. The later stages of the DNS suggest that for the turbulent state the computational box, in wall units, was 240 in x and 150 in y, as opposed to typical values from incompressible flow of 2000 and 1000, respectively.

Kral & Zang [47] have performed some LES of a Mach 4.5 turbulent boundary layer with computational domains closer to the standard incompressible sizes. Here they found that reasonable results could be obtained with the constants C_R closer to the accepted incompressible values. It appears that application of the dynamic eddy viscosity concept [37] to this problem would be quite fruitful.

The potential of LES for transition is that it permits computations through the transitional zone at an order of magnitude or more lesser expense than for DNS. A discussion of what sort of information can be reliably provided by LES and DNS is given in [48]. For incompressible flow, demonstrations are needed for spatial transition; for compressible flow, the role of the SGS viscosity needs clarification: To what extent is it furnishing artificial viscosity rather than serving its intended purpose of modeling the physics?

8 Prospects

The past several years have witnessed many exciting developments in transition research, particularly for compressible flow, that make an absolute amplitude criterion for prediction of transition onset a tantalizing prospect. Many of the components of such a methodology have been discussed in this paper. LST technology is virtually complete for real configurations. SIT is likely to be absorbed within PSE. The scope of PSE needs to be vastly increased and it would greatly benefit from a firmer mathematical foundation. DNS will no doubt undergo algorithmic improvements and take advantage of increased computational power. LES will likely evolve through several generations of SGS model improvements.

The philosophy, not only for transition prediction, but also for basic research into transition physics, ought to be to apply to each stage of transition or to each physical problem the most economical and revealing method in the transition prediction toolkit.

Acknowledgments

The authors would like to thank their many colleagues in the Theoretical Flow Physics Branch and at I.C.A.S.E. for their contributions to this work. The bulk of the SIT, PSE, DNS and LES results shown here were obtained during a 1990-91 special project on the NASA Ames Numerical Aerodynamic Simulation system. Special thanks go to Beyong Kim for the graphical illustration of the rope-like structures shown in Figure 12. The second and third authors were supported by NASA Langley Research Center under contracts NAS1-18240 and NAS1-18599, respectively.

References

[1] Smith, A. M. O.; and Gamberoni, A. H.: Transition, Pressure Gradient and Stability Theory. Report ES26388, Douglas Aircraft Co., 1956.

[2] Van Ingen, J. L.: A Suggested Semi-Empirical Method for the Calculation of the Boundary Layer Transition Region. Report VTH-74, Tech. Univ. Delft, Dept. of Aeronautics. 1956.

[3] Nishioka, M.; and Morkovin, M. V.: Boundary-layer receptivity to unsteady pressure gradients: experiments and overview. *J. Fluid Mech.* **171**:219-261, 1986.

[4] Goldstein, M. E.; and Hultgren, L. S.: Boundary-layer receptivity to long-wave free-stream disturbances. *Ann. Rev. Fluid Mech* **21**:137–166, 1989.

[5] Kerschen, E. G.: Boundary layer receptivity theory. *Appl. Mech. Rev.* **43**(5):S152-S157, 1990.

[6] Choudhari, M.; and Streett, C. L.: A Finite Reynolds Number Approach for the Prediction of Boundary Layer Receptivity in Localized Regions. NASA TM 102781, 1991.

[7] Choudhari, M.; and Streett, C.: Boundary Layer Receptivity Phenomena in Three-Dimensional and High-Speed Boundary Layers. *AIAA Paper No. 90-5258*, 1990.

[8] Choudhari, M., Ng, L.; and Streett, C. L.: A general approach for the prediction of localized instability generation in boundary layer flows. In *Proc. of the Boundary Layer Transition and Control Conference.* Cambridge, UK, April 9-12, 1991.

[9] Pruett, C. D., Ng., L., and Erlebacher, G.: On the nonlinear stability of a high-speed, axisymmetric boundary layer. *Phys. Fluids A* **3**, 1991, in press.

[10] Mack, L. M.: Boundary-layer linear stability theory. In *Special Course on Stability and Transition of Laminar Flow.* ed. R. Michel. AGARD Report No. 709, pp. 3.1-3.81, 1984.

[11] Pruett, C. D., Ng., L., and Erlebacher, G.: On the non-uniqueness of the parallel-flow approximation. In *Proc. of the ICASE/LaRC Workshop on Transition and Turbulence*, ed. M. Y. Hussaini. New York: Springer, 1992.

[12] El-Hady, N. M.: Nonparallel instability of supersonic and hypersonic boundary layers. *Phys. Fluids A* **3**(9):2164-2178, 1991.

[13] Malik, M. R.: Prediction and control of transition in supersonic and hypersonic boundary layers. *AIAA J.* **27**(11):1487-1493, 1989.

[14] Chang, C.-L.; Malik, M. R.; and Hussaini, M. Y.: Effects of Shock on the Stability of Hypersonic Boundary Layers. *AIAA Paper No. 90-1448*, 1990.

[15] Balakumar, M.; and Malik, M. R.: Waves Produced From a Harmonic Point Source in a Supersonic Boundary Layer. *AIAA Paper No. 91-1646*, 1991.

[16] Herbert, Th.: Secondary instability of boundary layers. *Ann. Rev. Fluid Mech.* **20**:487–526, 1988.

[17] El-Hady, N. M.: Spatial three-dimensional secondary instability of compressible boundary layer flows. *AIAA J.* **29**(5):688-696, 1991.

[18] Masad, J. A.; and Nayfeh, A. H.: Subharmonic instability of compressible boundary layers. *Phys. Fluids A* **2**(8):1380-1392, 1990.

[19] Ng, L.; and Erlebacher, G.: Secondary instabilities in compressible boundary layers. *Phys. Fluids A* **4**, 1992, in press.

[20] Ng, L. L.; and Zang, T. A.: Secondary Instability Mechanisms in Compressible, Axisymmetric Boundary Layers. *AIAA Paper No. 92-0748*, 1992.

[21] Bertolotti, F. P.: Linear and Nonlinear Stability of Boundary Layers with Streamwise Varying Properties. Ph.D. Dissertation, Ohio State University, 1990.

[22] Herbert, Th.: Boundary-Layer Transition – Analysis and Prediction Revisited. *AIAA Paper No. 91-0737*, 1991.

[23] Bertolotti, F.; and Herbert, Th.: Analysis of the linear stability of compressible boundary layers using the PSE. *Theor. Comput. Fluid Dyn.* **3**:117-124, 1991.

[24] Chang, C.-L.; Malik, M. R.; Erlebacher, G.; and Hussaini, M. Y.: Compressible Stability of Growing Boundary Layers Using Parabolized Stability Equations. *AIAA Paper No. 91-1636*, 1991.

[25] Kleiser, L.; and Zang, T. A.: Numerical simulation of transition in wall-bounded shear flows. *Ann. Rev. Fluid Mech.* **23**:495-537, 1991.

[26] Gilbert, N.; and Kleiser, L.: Near-wall phenomena in transition to turbulence. In *Near-Wall Turbulence: 1988 Zoran Zaric Memorial Conference*, ed. S.J. Kline & N.H. Afgan, pp. 7-28. Washington: Hemisphere, 1989.

[27] Rai, M. M.; and Moin, P.: Direct Numerical Simulation of Transition and Turbulence in a Spatially Evolving Boundary Layer. *AIAA Paper No. 91-1607*, 1991.

[28] Macaraeg, M. G.: Stability of nonsimilar shear layers. *Int. J. Numer. Meth. Heat & Fluid Flow*, 1992, in press.

[29] Pruett, C. D.; and Zang, T. A.: Direct Numerical Simulation of Laminar Breakdown in High-Speed, Axisymmetric Boundary Layers. *AIAA Paper No. 92-0742*, 1992.

[30] Atkins, H. L.: High-Order ENO Methods for the Unsteady Compressible Navier-Stokes Equations. *AIAA Paper No. 91-1557.*

[31] Fischer, M.; and Weinstein, L.: Cone transitional boundary-layer structure at $M_\epsilon = 14$. *AIAA J.* **10**:699-701, 1972.

[32] Kendall, J. M.: Wind tunnel experiments relating to supersonic and hypersonic boundary-layer transition. *AIAA J.* **13**:290–299, 1975.

[33] Demetriades, A.: Hypersonic Viscous Flow Over a Slender Cone. Part III: Laminar Instability and Transition. *AIAA Paper No. 74-535*, 1974.

[34] Galperin, B.; and Orszag, S. A. (eds.): *Large Eddy Simulation of Complex Engineering and Geophysical Flows.* Cambridge, UK: Cambridge Univ. Press, 1992, in press.

[35] Piomelli, U.; Zang, T. A.; Speziale, C. G.; and Hussaini, M. Y.: On the large eddy simulation of transitional wall-bounded flows. *Phys. Fluids A* **2**(2):257–265, 1990.

[36] Piomelli, U.; and Zang, T. A.: Large-eddy simulation of transitional channel flow. *Comput. Phys. Comm.* **65**:224-230, 1991.

[37] Germano, M.; Piomelli, U.; Moin, P.; and Cabot, W. H.: A dynamic subgrid-scale eddy viscosity model. *Phys. Fluids A* **3**(7):1760-1765, 1991.

[38] Zang, T. A.; and Piomelli, U. : Large-eddy simulation of transitional flow. In *Large Eddy Simulation of Complex Engineering and Geophysical Flows*, ed. B. Galperin and S. A. Orszag. Cambridge, UK: Cambridge Univ. Press, 1992, in press.

[39] Yoshizawa, A.: Statistical theory for compressible turbulent shear flows, with the application to subgrid modeling, *Phys. Fluids* **29**:2152-2164, 1986.

[40] Speziale, C. G.; Erlebacher, G.; Zang, T. A.; and Hussaini, M. Y.: The subgrid-scale modeling of compressible turbulence. *Phys. Fluids* **31**(4):940–942, 1988.

[41] Lesieur, M.; Comte, P.; and Normand, X.: Direct and Large–Eddy Simulations of Transitioning and Turbulent Shear Flows. *AIAA Paper No. 91-0335*, 1991.

[42] Moin, P.; Squires, K.; Cabot, W.; and Lee, S.: A Dynamic Subgrid–Scale Model for Compressible Turbulence and Scalar Transport, CTR Manuscript 124, 1991.

[43] Comte, P.; Lee, S.; and Cabot, W. H.: A subgrid–scale model based on the second–order velocity structure function. In *Proc. of the Summer Program 1990*, Center for Turbulence Research, pp. 31–45. Stanford University, 1990.

[44] Zang, T. A.; Dahlburg, R. B. and Dahlburg, J. P.: Direct and large–eddy simulations of three–dimensional compressible Navier–Stokes turbulence. *Phys. Fluids A* **4**(1), 1992, in press.

[45] Erlebacher, G.; Hussaini, M. Y.; Speziale, C. G.; and Zang, T. A.: Toward the large–eddy simulation of compressible turbulent flows. *J. Fluid Mech.* , 1992, in press.

[46] Piomelli, U.; Moin, P.; and Ferziger, J. H.: Model consistency in large–eddy simulation of turbulent channel flows. *Phys. Fluids* **31**:1884-1891, 1988.

[47] Kral, L. D.; and Zang, T. A.: Large-eddy simulation of supersonic, wall-bounded, turbulent flows In *Proc. of the ICASE/LaRC Workshop on Transition and Turbulence*, ed. M. Y. Hussaini. New York: Springer, 1992.

[48] Zang, T. A.: Numerical simulation of the dynamics of turbulent boundary layers: perspectives of a transition simulator. *Phil. Trans. R. Soc. Lond. A* **336**:95-102, 1991.